

A CO-to-H₂ ratio of $\approx 10^{-5}$ towards the Herbig Ae star HK Ori

P. WILSON CAULEY,¹ KEVIN FRANCE,² GREGORY J. HERZCEG,³ AND CHRISTOPHER M. JOHNS-KRULL⁴

¹Laboratory for Atmospheric and Space Physics, University of Colorado Boulder, 600 UCB, Boulder, CO 80303

²Laboratory for Atmospheric and Space Physics, University of Colorado Boulder, 600 UCB Boulder, CO 80303

³Kavli Institute for Astronomy and Astrophysics, Peking University, Yiheyuan Lu 5, Haidian Qu, 100871 Beijing, People's Republic of China

⁴Physics & Astronomy Department, Rice University, 6100 Main Street, Houston, TX 77005

(Received 12/18/2020; Accepted 02/24/2021)

Submitted to AAS journals

ABSTRACT

Measurements of gas mass in protoplanetary gas disks form the basis for estimating the conditions of planet formation. Among the most important constraints derived from disk diagnostics are the abundances of gas-phase species critical for understanding disk chemistry. Towards this end, we present direct line-of-sight measurements of H₂ and CO, employing UV absorption spectroscopy from *HST*-COS to characterize disk composition, molecular excitation temperatures, and spatial distribution in the circumstellar material around the Herbig Ae stars HK Ori and T Ori. We observe strong CO ($N(\text{CO}) = 10^{15.5} \text{ cm}^{-2}$; $T_{\text{rot}}(\text{CO}) = 19 \text{ K}$) and H₂ ($N(\text{H}_2) = 10^{20.34} \text{ cm}^{-2}$; $T_{\text{rot}}(\text{H}_2) = 141 \text{ K}$) absorption towards HK Ori with a CO/H₂ ratio ($\equiv N(\text{CO})/N(\text{H}_2)$) = $1.3^{+1.6}_{-0.7} \times 10^{-5}$. These measurements place direct empirical constraints on the CO-to-H₂ conversion factor in the disk around a Herbig Ae star for the first time, although there is uncertainty concerning the exact viewing geometry of the disk. The spectra of T Ori show CO ($N(\text{CO}) = 10^{14.9} \text{ cm}^{-2}$; $T_{\text{rot}}(\text{CO}) = 124 \text{ K}$) absorption. Interestingly, we do not detect any H₂ absorption towards this star ($N(\text{H}_2) < 10^{15.9} \text{ cm}^{-2}$). We discuss a potential scenario for the detection of CO without H₂, which deserves further investigation. The low abundance ratio measured around HK Ori suggests significant depletion of CO in the circumstellar gas, which conforms with the handful of other recent CO abundance measurements in protoplanetary disks.

1. INTRODUCTION

In the inner disks ($r < 10 \text{ AU}$) around young stars, molecular gas emission and absorption provide our best means of inferring the physical conditions at the radii where gas giant and rocky planet cores are forming and accreting their nascent atmospheres. The abundances of gas-phase species at the location of formation and accretion are expected to affect the chemical abundances of exoplanet atmospheres (Öberg et al. 2011). Recent surveys of molecular emission from Classical T Tauri Stars (CTTSs) and Herbig Ae stars have provided new constraints on the radial distribution, temperature, and composition of planet-forming disks. Surveys of mid-IR emission from CO (Salyk et al. 2009; Banzatti & Pontoppidan 2015), H₂O and organic molecules (Pontoppidan et al. 2010; Carr & Najita 2011), and spectrally/spatially-resolved near-IR observations (Pon-

toppidan et al. 2011; Brittain et al. 2015) have placed constraints on the CO and H₂O inventory at planet-forming radii and the evolution of the inner molecular gas disk radius (Antonellini et al. 2020). All of these studies require an accurate knowledge of the absolute abundances to convert these measurements into local gas masses.

An emerging consensus from ALMA observations of protoplanetary disks is that on large scales ($\sim 30 - 100 \text{ AU}$), CO is heavily depleted relative to H₂ (e.g., Miotello et al. 2017; Long et al. 2017). This depletion process may be fairly rapid, occurring within the first $\approx 1 \text{ Myrs}$ of a protostellar disk's lifetime (Zhang et al. 2020). When interpreted with physical-chemical models of disks that include CO freeze-out and photodissociation (Miotello et al. 2016), the ¹³CO line fluxes are much weaker than expected from dust emission and the few available detections of HD (Bergin et al. 2013; McClure et al. 2016), implying that something other than freeze-out is depleting the CO. The most plausible explanation is that complex C-bearing molecules also freeze-out in the disk mid-plane, although chemical reprocessing of CO in the cold

disk mid-plane is also possible for CTTS disks which are older than ≈ 1 Myr (Bosman et al. 2018). Once frozen out in a low-viscosity region, the ices will remain frozen out, with a time-dependence that will gradually deplete the disk of C and therefore CO (Kama et al. 2016; Schwarz et al. 2016).

Our best opportunity to converge on a three-dimensional view of the planet-forming regions around young stars, both inside and outside 10 AU, is to assemble a broad spectrum of relevant disk tracers and diagnostics (Sicilia-Aguilar et al. 2016). Among the most important items in this toolkit of disk diagnostics are measurements of the abundances and the physical conditions of the most important gas-phase species. Molecular absorption spectroscopy, where a pencil beam through the circumstellar disk is observed against the host star, provides a one-dimensional slice through the disk and allows the column density, temperature, and radial velocity of the absorbing gas to be quantified. This has historically been one of the most powerful techniques for diagnosing the composition and temperature structure of the ISM, and our approach in this work is to apply ultraviolet absorption spectroscopy techniques to better understand planet-forming environments around young stars.

UV absorption line spectroscopy has been used to measure CO around a number of CTTSs (McJunkin et al. 2013) and resulted in the first circumstellar CO/H₂ ratio for a pre-main sequence star (France et al. 2014a). UV spectroscopy cannot probe the disk mid-plane, but current models predict that carbon should rapidly get sequestered in solids in the disk mid-plane at all radii and not return to the gas phase. In the inner disk ($r \lesssim 4$ AU) the CO and H₂ in the warm molecular layer accounts for the vast majority of the carbon and hydrogen respectively (Ádámkóvics et al. 2014), which suggests that CO/H₂ measured through this region of the disk is a good approximation of the true CO/H₂ value.

The focus of this work is the circumstellar gas around the Herbig Ae stars T Ori and HK Ori. Both T Ori and HK Ori are well studied pre-main sequence systems. T Ori is a UX Orionis (UXOR) variable star which hosts a self-shadowed circumstellar disk (Hillenbrand et al. 1992; Hein Bertelsen et al. 2016) and has an estimated accretion rate of $\log(\dot{M}) = -6.58 \pm 0.40 M_{\odot} \text{ yr}^{-1}$ (Mendigutía et al. 2011a, however, see Section 4). The leading explanation for the UXOR phenomenon is the occultation of the central star by dust in the warped or puffed up inner disk rim (Dullemond et al. 2003; Kreplin et al. 2016). This requires that the disk be viewed nearly edge-on ($i \gtrsim 70^\circ$). Although no estimates of T Ori’s disk inclination angle exist, its nature as a UXOR and the SED evidence of a self-shadowed disk suggests that its disk is viewed at a large inclination angle. It also has a stellar rotational velocity of $v \sin i \approx 150 - 175 \text{ km s}^{-1}$ (Mora et al. 2001; Alecian et al. 2013; Cauley et al. 2015) implying that the star is viewed equatorially rather than pole-on.

HK Ori is also actively accreting from its circumstellar disk (Hillenbrand et al. 1992; Mendigutía et al. 2011a) with an accretion rate of $\log(\dot{M}) = -5.24 \pm 0.12 M_{\odot} \text{ yr}^{-1}$ and has a K4 binary companion at ≈ 150 AU, or $\approx 0''.3$ (Leinert et al. 1997; Baines et al. 2004; Smith et al. 2005; Wheelwright et al. 2010). There are no published constraints on the inclination angle of HK Ori’s circumstellar disk, although Blondel & Djie (2006) note that the low equivalent width of the Fe II 2400 Å absorption line suggests that we are viewing the star closer to pole-on since an edge-on orientation would produce a large Fe II equivalent width. Cauley et al. (2015) derived a projected rotational velocity of $v \sin i = 20 \text{ km s}^{-1}$ for HK Ori which is also indicative of a low inclination angle for the system. However, the spectrum of HK Ori is contaminated by a plethora of emission lines and there are few clean photospheric absorption lines which can be used to fit spectral templates. Thus the value from Cauley et al. (2015) should be viewed with caution. In addition, HK Ori shows significant spectroscopic and photometric variability (Eiroa et al. 2002; Baines et al. 2004; Mendigutía et al. 2011b) similar to the UXOR phenomenon although with smaller amplitude. Finally, HK Ori on average shows a double-peaked H α line profile with a strong central absorption feature (Reipurth et al. 1996; Mendigutía et al. 2011b; Cauley et al. 2015). This profile shape was shown to be qualitatively reproduced by accreting HAe stars viewed at high ($\gtrsim 70^\circ$) inclination (Muzerolle et al. 2004). The H α line profile variability also agrees well with the UXOR obscuration scenario tested by Muzerolle et al. (2004) for UX Ori. Overall, the evidence for a disk with a high inclination angle (i.e., edge-on disk) is stronger than for a low inclination angle.

In this paper we present new and archival *Hubble Space Telescope* FUV data for T Ori and HK Ori. We use the UV spectra to measure CO and H₂ column densities via pencil beam absorption through the circumstellar material and then compare the derived column densities to place constraints on the CO/H₂ ratios in the gas. Section 2 describes the UV spectroscopic data sets and Section 3 describes the spectral synthesis modeling used to derive molecular parameters. Section 4 places these results in context of current disk and interstellar sight-line studies and a brief summary of our findings is presented in Section 5.

2. OBSERVATIONS AND DATA REDUCTION

The data were collected in 2012 and 2019 as part of the HST Guest Observing Programs 12996 (P.I. Johns-Krull) and 15070 (P.I. France). Both HK Ori and T Ori were observed with two different Cosmic Origins Spectrograph (COS) settings in each program. The COS G130M $\lambda 1222$ setting from Program 15070 was selected to cover the wavelength range 1090 - 1360 Å which includes two H₂ $v = 0$ Lyman band transitions (Abgrall & Roueff 1989). We note that the G130M $\lambda 1291$ setting

from Program 12996 did not reach far enough into the blue to cover the relevant H_2 lines. Thus the H_2 analysis utilizes only the Program 15070 data. The G130M observations have a resolving power of $R \approx 16,000$, or a velocity resolution of $\Delta v = 19 \text{ km s}^{-1}$. HK Ori was observed for a total of $t = 7758$ seconds in this mode, while T Ori was observed for $t = 10089$ seconds.

The COS G160M $\lambda 1577$ setting covers the wavelength range 1400–1750 Å and contains the CO Fourth Positive $A-X$ system transitions from the $0 \leq v' \leq 4$ vibrational states. The G160M observations have a resolving power of $R \approx 18,000$, or a velocity resolution of $\Delta v = 17 \text{ km s}^{-1}$. HK Ori was observed for a total of $t = 1376$ seconds and T Ori was observed for $t = 1696$ seconds. All COS exposures were reduced with the standard calCOS pipeline.

Quality G160M spectra are available for T Ori from both 2012 and 2019 through both programs. The 2019 spectrum taken through Program 15070 has approximately double the amount of flux compared with the 2012 spectrum and the CO absorption is weaker by a factor of ≈ 2 . Interestingly, the flux ratio is roughly constant at ≈ 2 between the two epochs for wavelengths $\gtrsim 1300 \text{ Å}$ where the photosphere dominates but drops to ≈ 1 for wavelengths $\lesssim 1300 \text{ Å}$ where the accretion continuum likely dominates.

We have opted to use the 2012 spectrum in our analysis because of the more prominent CO feature. Although our choice to use the 2019 spectrum biases the CO analysis because of the stronger absorption seen in that epoch, the lack of H_2 in T Ori’s spectrum (see Section 3.1) prohibits any useful constraints on CO/ H_2 in the system. Thus the bias introduced does not influence any of our main conclusions concerning the circumstellar material around T Ori. We provide a more detailed discussion of T Ori’s FUV flux variability and how it might be related to the variable CO absorption and lack of H_2 absorption in Section 4.2.

Figure 1 show the final co-added spectra surrounding the H_2 Lyman band transitions of interest (Abgrall & Roueff 1989) and Figure 2 shows the final co-added spectra bracketing the CO $A-X$ band transitions. The spectra are smoothed with a 5-pixel boxcar. The UV spectra of many Herbig Ae/Be stars are littered with emission lines (e.g., Grady et al. 1996; Bouret & Catala 1998; Cauley et al. 2016), which are most clearly seen in HK Ori’s spectrum. In order to isolate the H_2 and CO absorption, we manually fit a high order spline, combined with a first or second degree polynomial, to the contaminating emission lines to estimate the “continuum” emission. The continuum fits in the 1090 – 1130 Å region are plotted as red lines in Figure 1.

For the 1400 – 1520 Å region containing the CO $A-X$ absorption bands, we compared the observed spectra to PHOENIX stellar photosphere models (Husser et al. 2013) to aid in identifying which features are stellar versus circumstellar. Scaled and reddened PHOENIX mod-

els are over-plotted in red in Figure 2. Note that HK Ori is a binary system with an A-type primary and G-type T Tauri secondary with a separation of $\approx 150 \text{ AU}$ (Leinert et al. 1997; Smith et al. 2005). We only show the A-type photosphere model in Figure 2 due to the much weaker flux of the G-type photosphere in the FUV. It is clear that the photosphere of HK Ori is dwarfed by the emission lines so the photosphere is relatively unimportant in this case. For T Ori, however, the spectrum from 1400 – 1520 Å is almost entirely due to the star’s photosphere with little, if any, excess accretion emission present. Thus we closely compared the photosphere model to the observed spectrum during the spline continuum fitting for T Ori so as to minimize the inclusion of stellar features in the final normalized CO spectrum. The excess CO absorption is fairly clear in most of the bandheads in Figure 2.

3. MODELING THE H_2 AND CO ABSORPTION

Calculating the CO/ H_2 ratio in the warm molecular layer of a disk requires a measurement of the co-spatial CO and H_2 densities. To accomplish this we model the column densities of H_2 and CO independently. The temperature of each gas is also derived independently. For the CO models, the rotational temperature is a model parameter; the H_2 rotational temperature is derived from the best-fit column densities in a separate fitting procedure. All model spectra are convolved with the COS linespread-function (LSF) (Kriss 2011), which varies as a function of wavelength.

3.1. H_2 models

The $v'' = 0, J''$ H_2 absorption lines are fit using the *h2ools* suite of optical depth templates from McCandliss (2003), which contain all of the Lyman and Werner transitions from the ground vibrational level of the electronic ground state (Abgrall & Roueff 1989). Each template spectrum is calculated for an integer value of the Doppler parameter b , where $b = (2kT_{\text{rot}}/m_{\text{H}_2} + v_{\text{turb}}^2)^{1/2}$, and assuming a column density of $N = 10^{21} \text{ cm}^{-2}$. The free parameters in the fit are the line-of-sight radial velocity of the absorbing gas v_{rad} , the coverage fraction of the stellar disk by the gas f_{cov} , the Doppler broadening parameter b , and the column densities of the rotational transitions $J'' = 0 - 8$. We note that although the velocity resolution of the observations is $\approx 17 \text{ km s}^{-1}$, the value of b can be constrained at much higher precision since it has a strong effect on the optical depth of the unsaturated H_2 transitions. Because the templates from McCandliss (2003) are optical depth vectors, and the optical depth is proportional to the column density, the templates can be adjusted for any column density by multiplying by $N/10^{21}$. The absorption spectrum is then computed as $e^{-\tau_i}$ where τ_i is the value of the scaled optical depth template at each wavelength. Rotational transitions $J'' > 8$ are not seen in the data and thus we exclude them from the modeling.

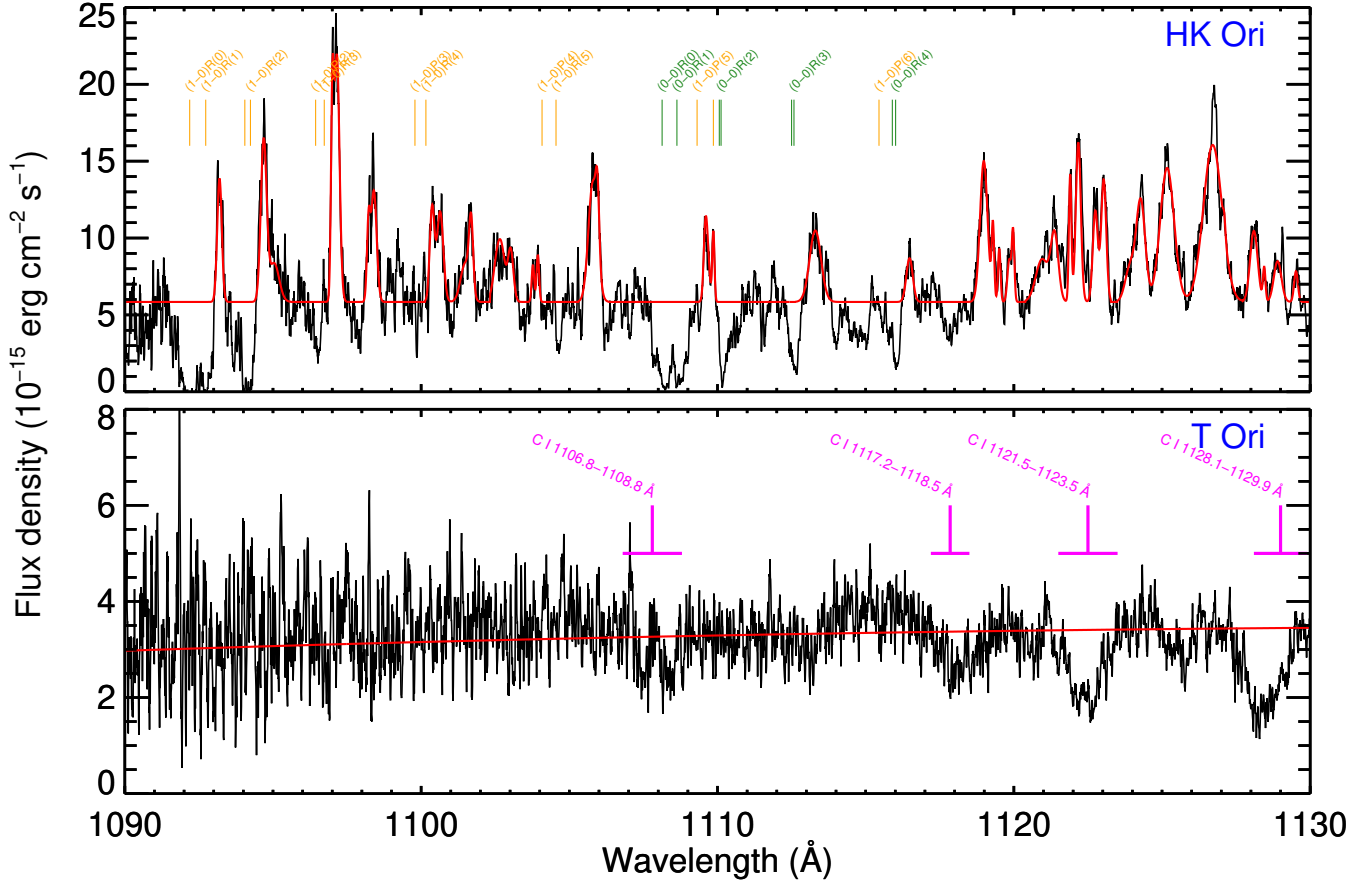


Figure 1. Extracted G130M spectra in the surrounding region of the H₂ Lyman band. The observed spectra are shown in black and the continuum fits in red. Transitions to $v' = 0$ are marked in green and transitions to $v' = 1$ are marked in orange. Transition labels for (1-0)P(1) at 1094.05 Å, (1-0)R(6) at 1109.86 Å, (0-0)P(1) at 1110.06 Å, (0-0)P(2) at 1112.50 Å, and (0-0)P(3) at 1115.90 Å are omitted for clarity. Clear absorption is visible in the HK Ori spectrum while the T Ori spectrum shows no sign of absorption by H₂. The absorption features in the T Ori spectrum are C I lines, most of which are likely accretion-related.

We perform the model fits using our custom MCMC routine based on the algorithm of Goodman & Weare (2010) (see also Foreman-Mackey et al. 2013). Uniform priors are assumed for all parameters. We run the MCMC for 10,000 steps with 100 walkers, resulting in 10^6 samplings of the posterior distribution. Because the template spectra are calculated for discrete values of b we interpolate between the two templates which bracket the model value of b . For example, if the MCMC iteration requires a spectrum with $b = 3.2 \text{ km s}^{-1}$ we linearly interpolate between the $b = 3.0 \text{ km s}^{-1}$ and $b = 4.0 \text{ km s}^{-1}$ templates. Once the interpolation is complete the resulting spectrum is shifted by the radial velocity and scaled to find the best-fit column density. The model spectrum, which is at the native velocity resolution, is convolved with the COS LSF for comparison with the observed spectrum. The median values of the marginalized posterior distributions are taken as the best-fit parameter values and the 1σ confidence intervals are the 16th and 84th percentiles of the marginalized posteriors.

For T Ori there is no visual evidence of H₂ absorption (see Figure 1 and Figure 5) and the spectrum from 1090–1130 Å is almost pure continuum (surprising given the strong CO detection, discussed in the following section). We apply the above H₂ fitting procedure to T Ori’s spectrum, with some exceptions, to measure the upper limit to T Ori’s H₂ absorption properties. For T Ori we fix the coverage fraction at $f_{\text{cov}} = 1.0$ and we freeze the radial velocity near a literature value for the system of $v_{\text{rad}} = 56.0 \text{ km s}^{-1}$ (Cauley & Johns-Krull 2015). This is necessary because the lack of absorption lines in the spectrum allows a total degeneracy between f_{cov} and the H₂ column densities. For the same reason v_{rad} is entirely unconstrained.

The marginalized posterior distributions from the MCMC are shown for HK Ori in Figure 3 and for T Ori in Figure 4. Darker blue colors indicate regions of higher posterior density. The fixed parameters for T Ori f_{cov} and v_{rad} are excluded from Figure 4. We also exclude the posteriors for the rotational states $J'' = 7, 8$

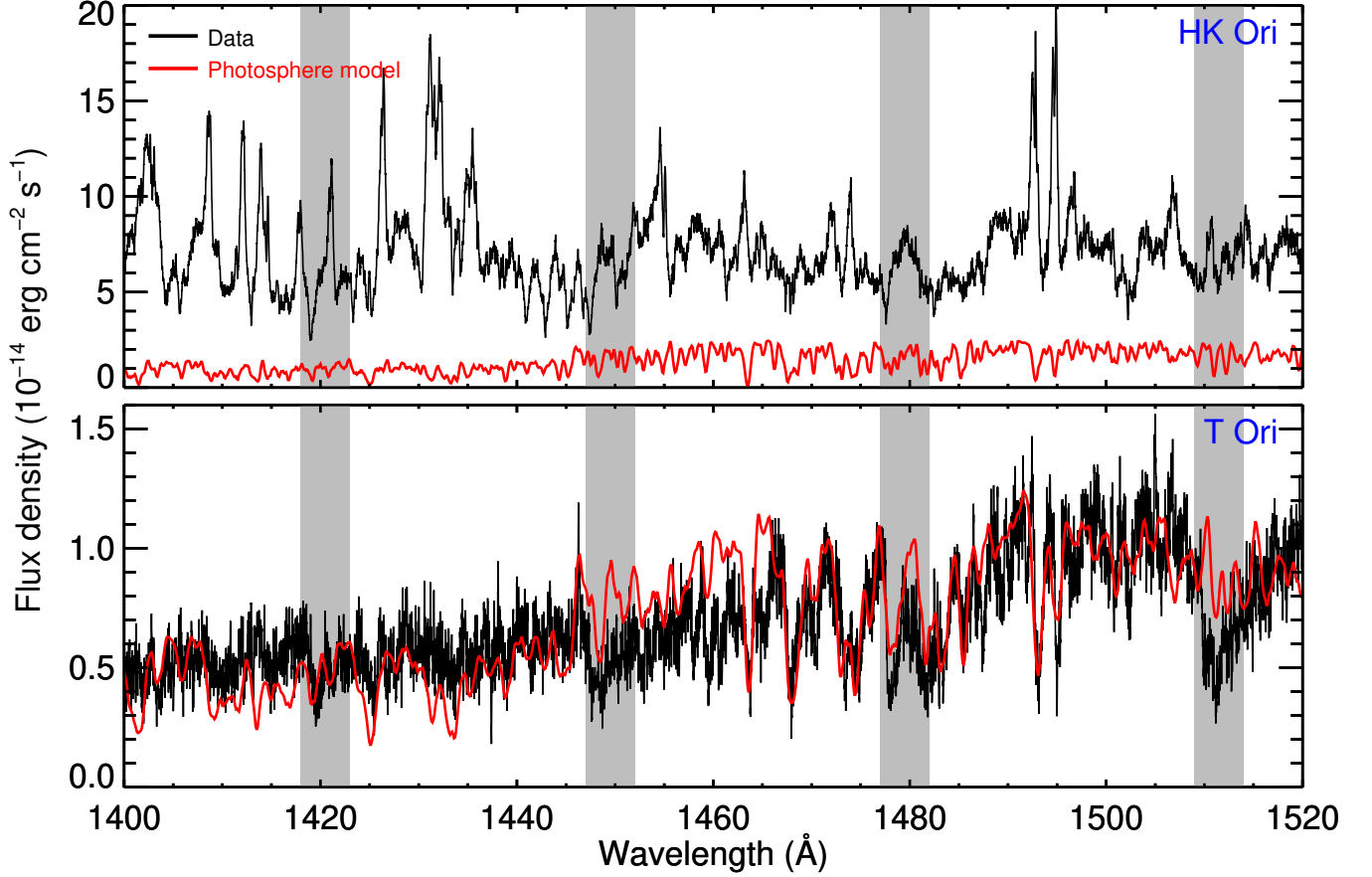


Figure 2. Extracted G160 M spectra in the surrounding region of the CO Fourth Positive system. The stellar spectra are shown in black and scaled photosphere models from PHOENIX are shown in red. The photospheric models are used as a guide to which features are stellar versus circumstellar. The wavelength segments containing the CO A – X bands are shaded in gray.

for both objects due to severe blending of the $J'' = 7$ state and no detectable features corresponding to the $J'' = 8$ state.

The most likely model parameters and their 1σ confidence intervals are given in Table 1 and the best-fit models are shown in Figure 5. As expected, we are only able to place an upper limit on the H_2 column density for T Ori due to the lack of any discernible H_2 absorption in the spectrum. Also over-plotted for T Ori in Figure 5 is the expected H_2 absorption assuming the canonical interstellar dense and translucent cloud ratios ($\text{CO}/\text{H}_2 = 10^{-4}$ and $= 10^{-5}$) and temperature $T_{\text{rot}} = 125$ K where the temperature and CO column density are those derived in Section 3.2. A model with such a large H_2 column density is strongly ruled out by the MCMC posteriors. We will return to potential explanations for the lack of circumstellar H_2 absorption around T Ori in Section 4.

The most likely parameter values for HK Ori, on the other hand, give a total H_2 column density of $\log_{10}(N[\text{H}_2]) = 20.34^{+0.03}_{-0.03} \text{ cm}^{-2}$. The broadening parameter value is $b = 4.9^{+0.58}_{-0.60} \text{ km s}^{-1}$ suggesting a significant

Table 1. H_2 model fit parameters

Parameter	HK Ori	T Ori
(1)	(2)	(3)
$N(J'' = 0)^\dagger \text{ (cm}^{-2}\text{)}$	$20.17^{+0.04}_{-0.04}$	$15.8^{+1.0}_{-2.8}$
$N(J'' = 1) \text{ (cm}^{-2}\text{)}$	$19.80^{+0.04}_{-0.04}$	<15.5
$N(J'' = 2) \text{ (cm}^{-2}\text{)}$	$18.85^{+0.13}_{-0.17}$	<14.3
$N(J'' = 3) \text{ (cm}^{-2}\text{)}$	$17.44^{+0.30}_{-0.31}$	<14.4
$N(J'' = 4) \text{ (cm}^{-2}\text{)}$	$16.75^{+0.35}_{-0.30}$	<13.7
$N(J'' = 5) \text{ (cm}^{-2}\text{)}$	$16.12^{+0.48}_{-0.35}$	<13.9
$N(J'' = 6) \text{ (cm}^{-2}\text{)}$	$11.71^{+1.33}_{-1.23}$	<13.5
$N(J'' = 7) \text{ (cm}^{-2}\text{)}$
$N(J'' = 8) \text{ (cm}^{-2}\text{)}$	$12.58^{+1.59}_{-1.85}$	<15.5
$v_{\text{rad}} \text{ (km s}^{-1}\text{)}$	$-19.9^{+0.9}_{-0.9}$	56.0
$b \text{ (km s}^{-1}\text{)}$	$4.9^{+0.58}_{-0.60}$	$2.1^{+3.8}_{-0.8}$
f_{cov}	$0.995^{+0.004}_{-0.007}$	1.0
$T_{\text{rot}} \text{ (K)}$	141^{+6}_{-6}	452^{+649}_{-178}

† All column densities N are \log_{10} values.

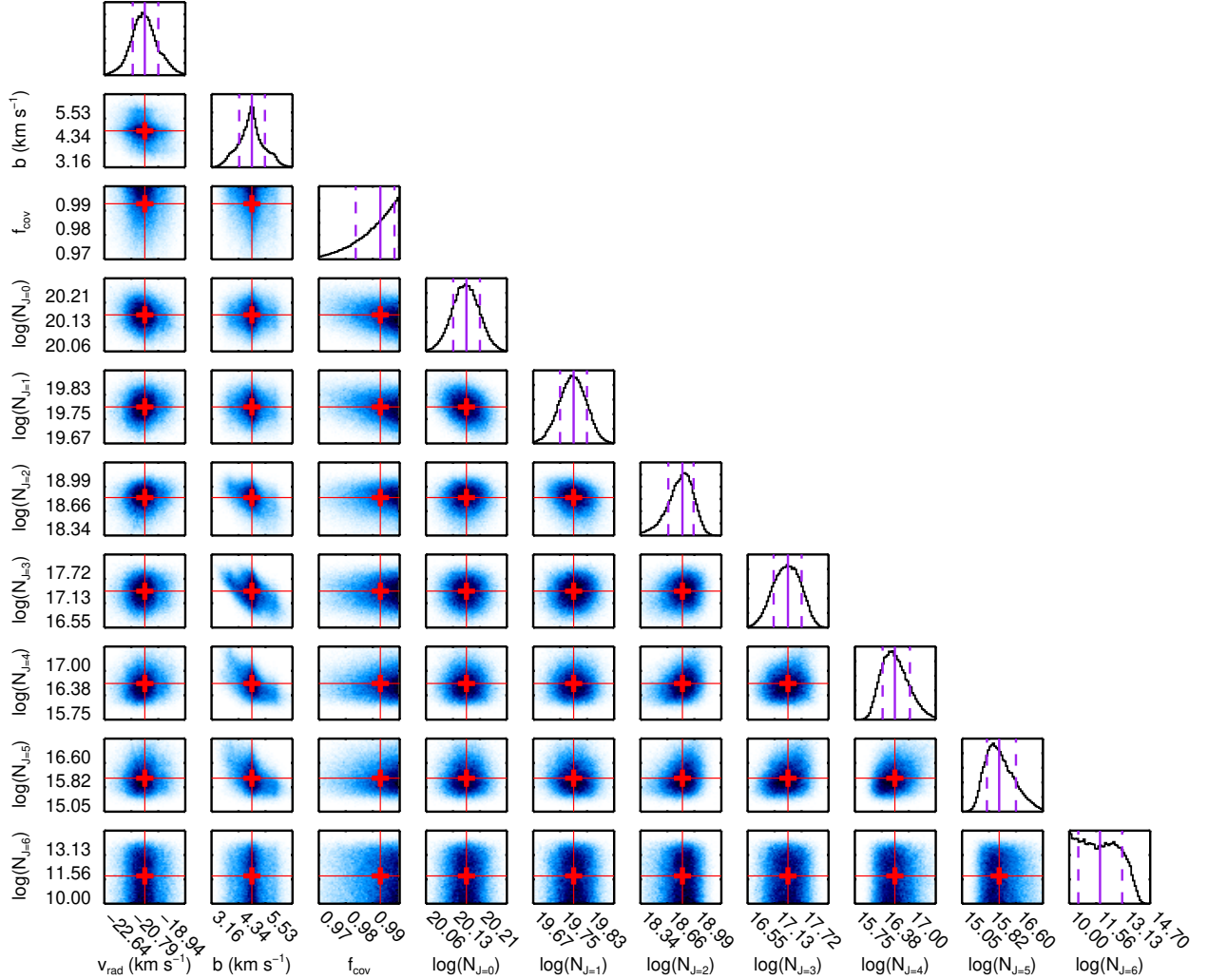


Figure 3. Corner plot of the marginalized posterior distributions for the H₂ MCMC of HK Ori. Note that all column densities N are in units of cm^{-2} .

contribution from turbulence or unresolved components to the line widths. The model also indicates that the H₂ line-of-sight absorption covers the entire stellar disk given the value of f_{cov} so close to 1.0.

The temperature of the H₂ is not a free parameter in the spectrum fitting. Instead, we use the derived column densities to find the most-likely rotational temperature. The low- J'' H₂ level populations in the disk are expected to be determined by collisions so we can calculate the temperature of the gas assuming a Maxwell-Boltzmann distribution of the rotational states (see France et al. 2014a). We accomplish this by using the same MCMC routine to fit a line to the H₂ densities as a function of the excitation temperature of the various rotational states. The rotational, or kinetic, temperature T_{rot} of the gas is then the slope of the best-fit line.

The most-likely linear fit is shown with a red line in Figure 6 along with one hundred models from a random

sampling of the accepted posterior distributions (gray lines). We find that the H₂ gas around HK Ori has a rotational temperature of $T_{\text{rot}} = 142^{+6}_{-6}$ K. The small fit uncertainties on the $J'' = 0, 1, 2$ dominate the slope fit and thus the temperature determination. As expected from the lack of any H₂ absorption around T Ori, the corresponding temperature fit is mostly unconstrained: the same procedure yields $T_{\text{rot}} = 452^{+649}_{-178}$ K for T Ori.

3.2. CO models

The CO fitting procedure is outlined in detail in McJunkin et al. (2013) (see also France et al. 2014a) and we briefly summarize the salient points here. To derive the circumstellar CO column densities we fit the CO Fourth Positive band system shaded in gray in Figure 2. We include the (4–0), (3–0), and (2–0) bands in the fits for both objects but exclude the (1–0) band for the HK Ori fit due to contamination by what is most likely an

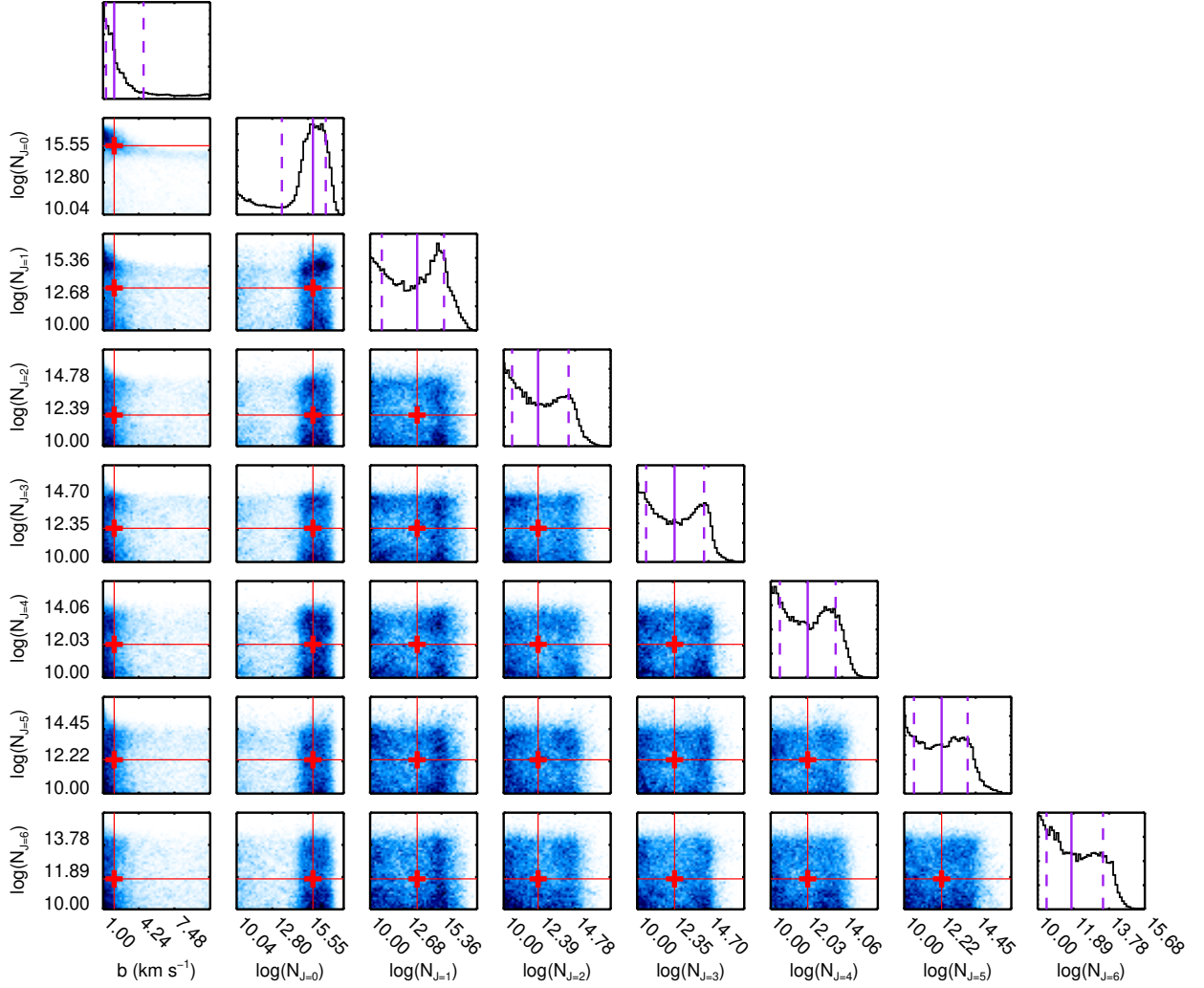


Figure 4. Corner plot of the marginalized posterior distributions for the H_2 MCMC of T Ori. The parameters are almost entirely unconstrained due to the lack of absorption in the observed spectrum.

emission line from atomic iron. The synthetic CO spectra are generated using literature oscillator strengths and ground-state energy levels (Haridass & Huber 1994; Eidelsberg et al. 1999; Eidelsberg & Rostas 2003). The free parameters in the MCMC fitting procedure are the column densities of ^{12}CO and ^{13}CO , the radial velocity of the absorbing gas v_{rad} , the rotational temperature of the gas T_{rot} , and the Doppler-broadening parameter b . Similar to the case for H_2 , b has a strong affect on the optical depth of the CO transitions and is somewhat degenerate with the column density. This makes the value of b sensitive to not only the line widths but the line depths as well.

We again adopt uniform, non-restrictive priors for most of the parameters and run the 100 walkers for 10,000 steps each. The one exception is the Doppler broadening parameter b : we restrict the prior range to $0.0 < b \leq 5.0 \text{ km s}^{-1}$. For each model iteration we

generate the CO spectrum using the input T_{rot} , b , and column density values. The spectrum is then shifted in velocity space according to v_{rad} and then convolved with the COS LSF to produce the output model.

The marginalized posterior distributions for the CO MCMC fits are shown in Figure 7 and Figure 8. The best-fit models (red) and fifty random samplings of the accepted posteriors (green) are shown in Figure 9. The most noticeable difference in the CO spectra is the width of the absorption bands, where HK Ori's are fairly narrow while T Ori's are broad. This is manifested in the large difference in derived T_{rot} values: for HK Ori $T_{\text{rot}} = 19_{-6}^{+11} \text{ K}$ and for T Ori $T_{\text{rot}} = 124_{-44}^{+53} \text{ K}$. Note that T Ori's b -value is just the median of the prior range, i.e., it is unconstrained. This is a result of the high temperature: as the temperature increases and the optical depth in the higher rotational states increases, the individual line broadening becomes less important and the instru-

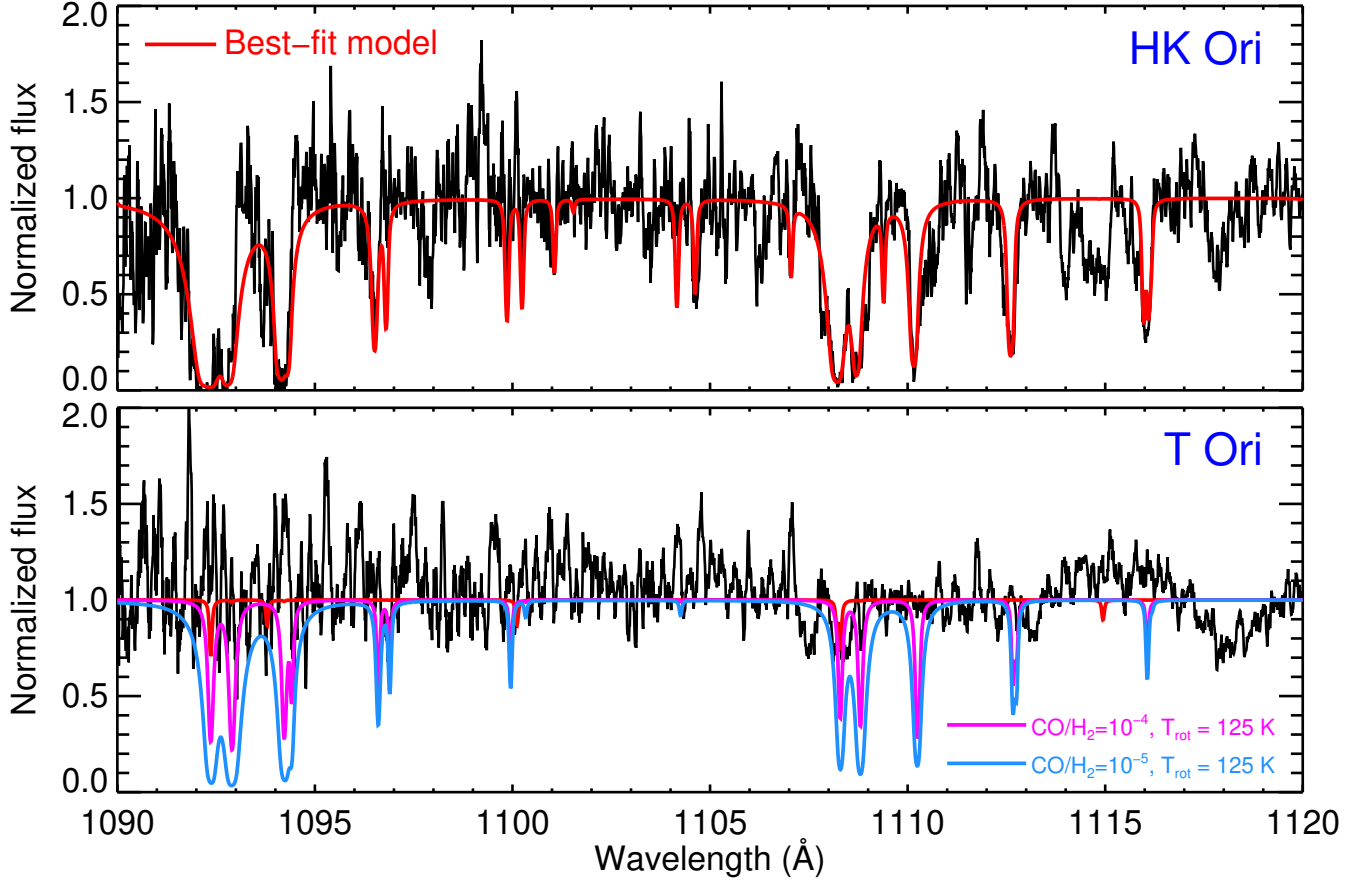


Figure 5. Normalized *HST* COS spectra of HK Ori (top) and T Ori (bottom) from 1090 – 1120 Å. The best-fit H₂ absorption models are over-plotted in red. No significant H₂ absorption is detected in the spectrum of T Ori. The magenta model shows the expected H₂ absorption assuming a conservative CO/H₂ ratio of 10^{−4} and the same temperature as that derived for the CO gas (see Section 3.2). The blue model shows an assumed ratio of 10^{−5}.

mental profile makes differences in b negligible. This is not the case for the low temperature fits for HK Ori. At low temperatures larger values of b increase the optical depth over a narrow range of rotational states which significantly increases the absorption depth. Thus there is some degeneracy between N and b at low T and b is constrained even though it is much smaller than the instrumental resolution. Neither spectrum shows any strong absorption due to ¹³CO, in contrast to some CTTS disks (e.g. France et al. 2012).

We note that the ¹²CO/¹³CO ratios indicated by our analysis are much larger than is typically found for the ISM or the circumstellar environments of young stellar objects (YSOs) (Smith et al. 2015). However, the ¹³CO column densities are highly uncertain and it’s likely that the ¹³CO absorption is almost entirely lost in the noise for both objects. Thus we caution against applying the derived ¹²CO/¹³CO ratios to further work on these systems.

3.3. H I Absorption

Table 2. CO model fit parameters

Parameter	HK Ori	T Ori
(1)	(2)	(3)
$N(^{12}\text{CO})^\dagger$ (cm ^{−2})	$15.5^{+0.3}_{-0.3}$	$14.9^{+0.2}_{-0.1}$
$N(^{13}\text{CO})$ (cm ^{−2})	$11.0^{+2.6}_{-4.2}$	$9.2^{+3.1}_{-3.0}$
v_{rad} (km s ^{−1})	$-14.9^{+4.1}_{-4.6}$	$44.5^{+6.7}_{-5.1}$
b (km s ^{−1})	$1.1^{+0.3}_{-0.2}$	$2.5^{+1.7}_{-1.4}$
T_{rot} (K)	19^{+11}_{-6}	124^{+53}_{-44}

[†] Column densities N are log₁₀ values.

Absorption line analyses of interstellar sight-lines often rely on a knowledge of the total neutral hydrogen column density, $N(\text{H I})$, to place molecular absorption properties in context. Toward this end, we use the 2012 *HST*-COS G130M observations of both stars to measure $N(\text{H I})$ by fitting the Ly α absorption profile. We show the observed profiles and reconstructed spectra from the model fits in Figure 10. Both HK Ori and T

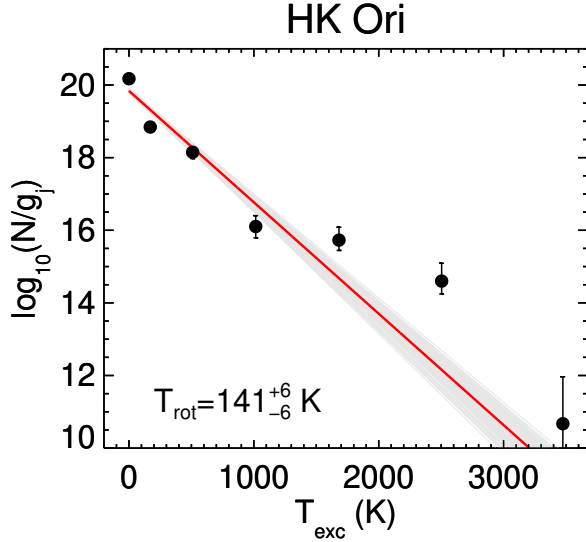


Figure 6. Fit to the H₂ excitation temperature versus column density for HK Ori. One hundred random samplings of the posterior distributions are shown in gray. The best-fit value for the rotational excitation temperature is $T_{\text{rot}} = 141^{+6}_{-6}$ K, indicative of material in a warm disk layer.

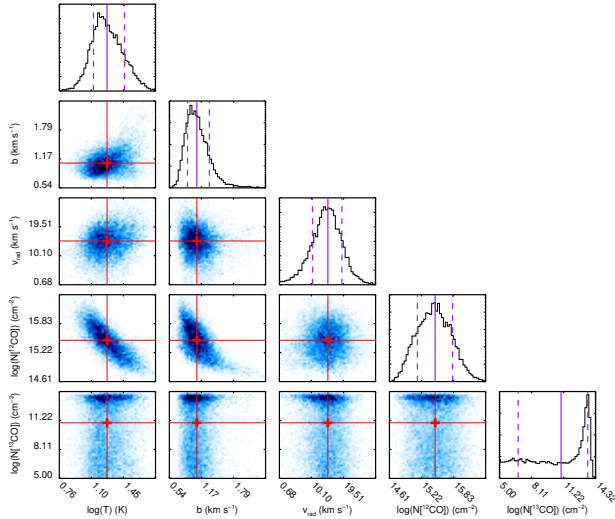


Figure 7. Corner plot of the marginalized posterior distributions for the CO MCMC of HK Ori.

Ori display broad Ly α emission features consistent with accretion-generated H I emission observed on lower mass T Tauri stars (e.g., France et al. 2014b). In analogy to the methodology employed for H₂ and CO, we assume the observed profile is the superposition of an underlying stellar emission spectrum and the Ly α absorber. For HK Ori, we employed a broad Gaussian as the intrinsic Ly α profile shape, and implemented an iterative fitting routine to find the best fit to the observed COS G130M Ly α spectra (France et al. 2012; McJunkin et al.

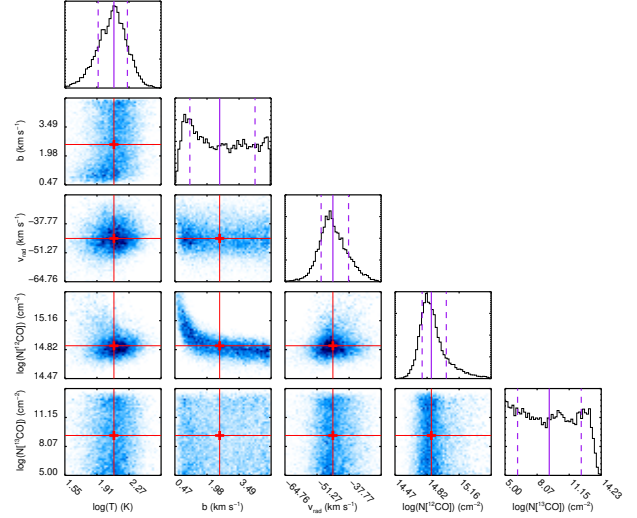


Figure 8. Corner plot of the marginalized posterior distributions for the CO MCMC of T Ori.

2013). The Ly α emission peak is less pronounced in T Ori, and here we fit a spline function to the continuum and emission line as a baseline for fitting the H I absorption. The Doppler b -value, b_{HI} , is assumed to be 10 km s⁻¹ for both stars. For more details on reconstructing intrinsic Ly α profiles see McJunkin et al. (2014).

For HK Ori, our fits find a baseline continuum of 8×10^{-15} erg cm⁻² s⁻¹ Å⁻¹, Gaussian peak amplitude of 6×10^{-12} erg cm⁻² s⁻¹ Å⁻¹, a Gaussian FWHM = 1100 km s⁻¹, and $\log_{10}N(\text{H I}) = 20.75 \pm 0.10$. Taking the spline function as the underlying stellar spectrum for T Ori, we find $\log_{10}N(\text{H I}) = 20.25 \pm 0.10$. These results are summarized in Table 3.

4. DISCUSSION

4.1. Comparing H₂, CO, and H I with the Translucent ISM

We compared the absorption properties of the two targets against typical properties of interstellar sightlines to help solidify assignment of these components to a circumstellar disk origin. The HK Ori CO/H₂ ratio and molecular fraction¹ are consistent with interstellar clouds at the diffuse-to-translucent boundary (e.g., Burgh et al. 2007). However, the CO and molecular fraction are considerably higher than expected for a star with HK Ori's optical reddening $E(B - V)$ (= 0.12; assuming the $N(\text{H I})$ to reddening conversion from Diplas & Savage 1994). Furthermore, the H₂ column density to HK Ori is orders of magnitude higher than what is seen to typical hot star targets near the Orion star-forming

¹ The molecular fraction, f_{H_2} is defined as $f_{\text{H}_2} = 2N(\text{H}_2)/(2N(\text{H}_2) + N(\text{H I}))$.

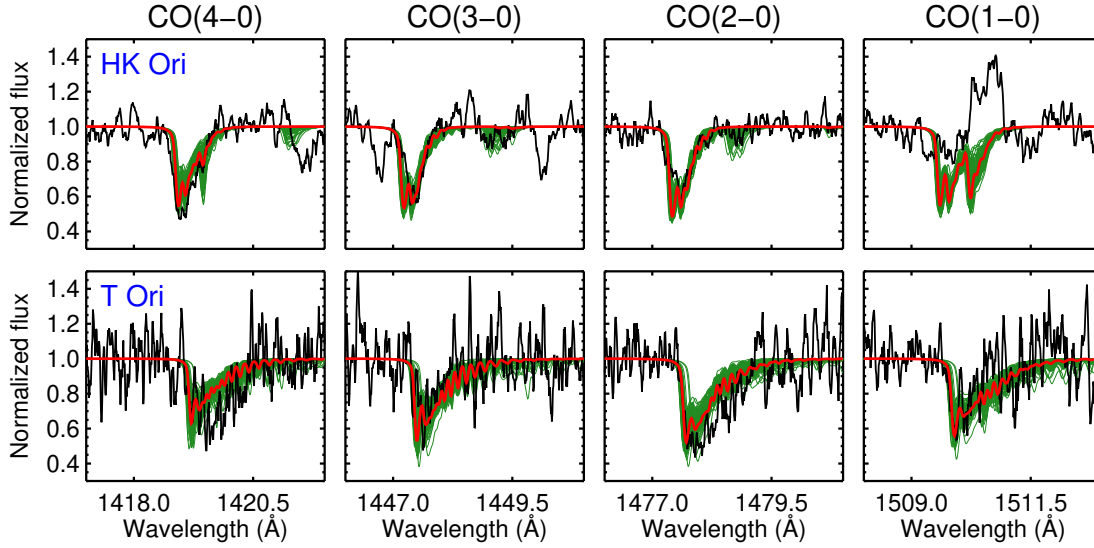


Figure 9. Normalized spectra surrounding the CO ($A-X$) absorption bands for HK Ori (top row) and T Ori (bottom row). The best-fit CO absorption models are over-plotted in red and one hundred random draws from the accepted posterior chains are shown in green. Note that the CO(1-0) band is excluded from the model determination for HK Ori due to the contamination by the strong emission line near 1511 Å.

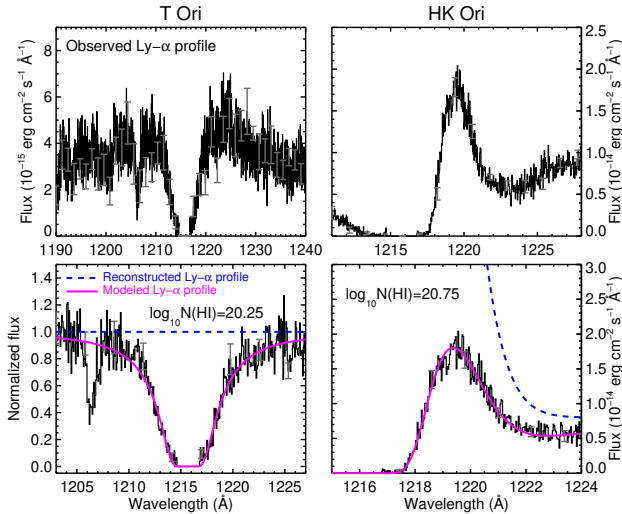


Figure 10. Observed (top panels) and reconstructed (bottom panels) Ly α profiles for T Ori and HK Ori. The best-fit neutral hydrogen ISM column densities are labeled in the bottom panels.

region (Savage et al. 1977). This points to a circumstellar origin of the molecular gas in HK Ori.

Further support for a circumstellar origin of the molecular gas around HK Ori comes from an analysis of the excitation temperatures. While $T(\text{H}_2) = 141$ K is con-

sistent with an interstellar origin, $T(\text{CO}) = 19$ K is much higher than what is seen for translucent clouds (e.g., see Figure 6 of Burgh et al. 2007). We note that the temperature discrepancy could be due to the density of CO being below the critical density (see Section 4.4 for a more detailed explanation). Therefore, numerous lines of evidence suggest a circumstellar, as opposed to interstellar, origin for the molecular gas observed toward HK Ori.

T Ori’s hydrogen sightline is characteristic of hot stars near the Orion star forming regions ($N(\text{H}_2) < 10^{16} \text{ cm}^{-2}$; $N(\text{H I}) = 10^{20.0-20.5} \text{ cm}^{-2}$; Savage et al. 1977). However, the diffuse sightlines in Orion are typically associated with very low CO upper limits ($N(\text{CO}) < 10^{13} \text{ cm}^{-2}$; Federman et al. 1980). Similarly, the very low molecular fraction is incompatible with the large CO column density, arguing that the CO we observe towards T Ori is almost certainly of a circumstellar origin. This is corroborated by the high $T(\text{CO})$, which is a factor of $\sim 10 - 20$ higher than seen on translucent interstellar sight-lines (Burgh et al. 2007; Sheffer et al. 2008). The circumstellar nature of T Ori’s CO absorption is also bolstered by the fact that it shows a variable column density likely related to inner disk material (see Section 4.2).

4.2. Where’s the H_2 around T Ori?

The lack of H_2 absorption towards T Ori is surprising given the system’s young age and the high likelihood that we observe the disk closer to an edge-on orientation.

Table 3. Total column densities and $N(\text{CO})/N(\text{H}_2)$ ratios

Object	$N(\text{H}_2)$	$N(\text{CO})$	$N(\text{H I})$	$N(\text{CO})/N(\text{H}_2)$	f_{H_2}
(1)	(2)	(3)	(4)	(5)	(6)
HK Ori	$20.34^{+0.03}_{-0.03}$	$15.5^{+0.5}_{-0.2}$	20.75 ± 0.10	$1.3^{+1.6}_{-0.7} \times 10^{-5}$	0.44
T Ori	$< 15.9^{+1.0}_{-0.4}$	$14.9^{+0.2}_{-0.1}$	20.25 ± 0.10	...	$< 1 \times 10^{-4}$

The properties of the CO gas we derive confirm that the gas is circumstellar ($T \approx 125$ K) and not interstellar, where the gas typically has temperatures $T < 10$ K. Furthermore, the radial velocity of the CO absorption, $\approx 45 \text{ km s}^{-1}$, is consistent with, although mildly blue-shifted relative to, the system velocity of $\approx 56 \text{ km s}^{-1}$ (noting that *HST*-COS has a wavelength accuracy of 15 km s^{-1}).

We can look to the variability between the 2012 and 2019 observations for clues about the lack of H_2 absorption towards the star. In Figure 11 we show a comparison between the *HST* COS spectra from 2012 (red) and 2019 (purple). The bottom panel shows the raw spectra for wavelengths common to both epochs and the middle panel shows the ratio of the fluxes. The top panel displays zoomed-in normalized comparisons between strong spectral features. A few things are evident from Figure 11: 1. The flux at wavelengths longer than $\approx 1300 \text{ \AA}$ was $\approx 2\times$ greater in 2019 than in 2012; 2. The flux at wavelengths shorter than $\approx 1300 \text{ \AA}$ stayed relatively constant; 3. Most of the photospheric absorption lines are weaker when the star is fainter; 4. The CO absorption is stronger when the star is fainter (see the flux dips within the gray bands in the middle panel of Figure 11). Additionally, we downloaded *V*-mag ASAS-SN light curves (Shappee et al. 2014; Kochanek et al. 2017) of T Ori and interpolated the observed magnitudes onto our *HST* COS observation dates: for the 2012 observations $V \approx 11.3$ and for the 2019 observations $V \approx 10.4$, which translates to a factor of ≈ 2.3 in flux. The *V*-band measurements confirm that the optical flux varies at a similar level to the FUV flux.

We speculate that T Ori’s nature as a rapid rotator and UXOR variable can qualitatively explain the phenomena seen in Figure 11. First, rapidly rotating stars are subject to non-negligible gravity darkening where the oblateness of the star causes the poles to be hotter than the equator (von Zeipel 1924; Espinosa Lara & Rieutord 2011). If the UXOR screen preferentially blocks equatorial stellar latitudes, or is at least more optically thick across these regions, the star will be dimmer but the stellar spectrum will be weighted towards the hotter polar regions. This can account for the observed shallower absorption lines in the 2012 faint phase. Second, the increased CO absorption during the faint phase could be a result of the increased gas column density produced by the occulting screen. Finally, the lack

of H_2 absorption in the Lyman transitions may be the result of the sub-1300 \AA flux, which is related to material accreting onto the star, being scattered into the line-of-sight over a large volume in the inner disk region. If the flux is the result of scattering over a large volume, we are not probing the same pencil beam through the disk that produces the CO absorption since the flux from 1400 - 1500 \AA is largely photospheric in origin. This also explains the relatively stable sub-1300 \AA flux since the UXOR screen does not occult the entire scattering surface.

We stress that the scenario outlined above is speculative; there are likely other plausible explanations for the various phenomena (e.g., an occulting accretion column and related veiling of the stellar photosphere). In particular, the proposed viewing geometry must be fine-tuned in order to preferentially occult equatorial latitudes on the star, leaving the hotter poles visible. Additional FUV time-series spectra will be useful in determining a more precise view of the system geometry and we defer a more quantitative characterization of the variability to future work.

4.3. Large Doppler broadening parameters

The H_2 and CO analysis for HK Ori suggest large ($\approx 1 - 4 \text{ km s}^{-1}$) non-thermal broadening components are necessary to reproduce the observed H_2 and CO absorption. This would imply significant contributions from turbulence or spatially unresolved gas motions responsible for the line broadening. The turbulence interpretation seems unlikely given that CO radio observations suggest that turbulence in protoplanetary disks is weak at distances of $\approx 10\text{s}$ of AU (Hughes et al. 2011; Flaherty et al. 2018, 2020). On the other hand, the pencil beam H_2 observations, if passing through the disk, likely probe higher surface layers than the thermal CO emission.

We caution against an over-interpretation of the large value for the Doppler parameter for two reasons. First, absorption features with widths of a few kilometers per second are not resolved in our spectra. The large b -values are mainly a result of the models fitting the absorption line depths, which are determined by both b and the column density N . Without resolving the line widths of individual H_2 and CO transitions it is difficult to say with confidence what is driving the large values of b . Second, there is considerable uncertainty around

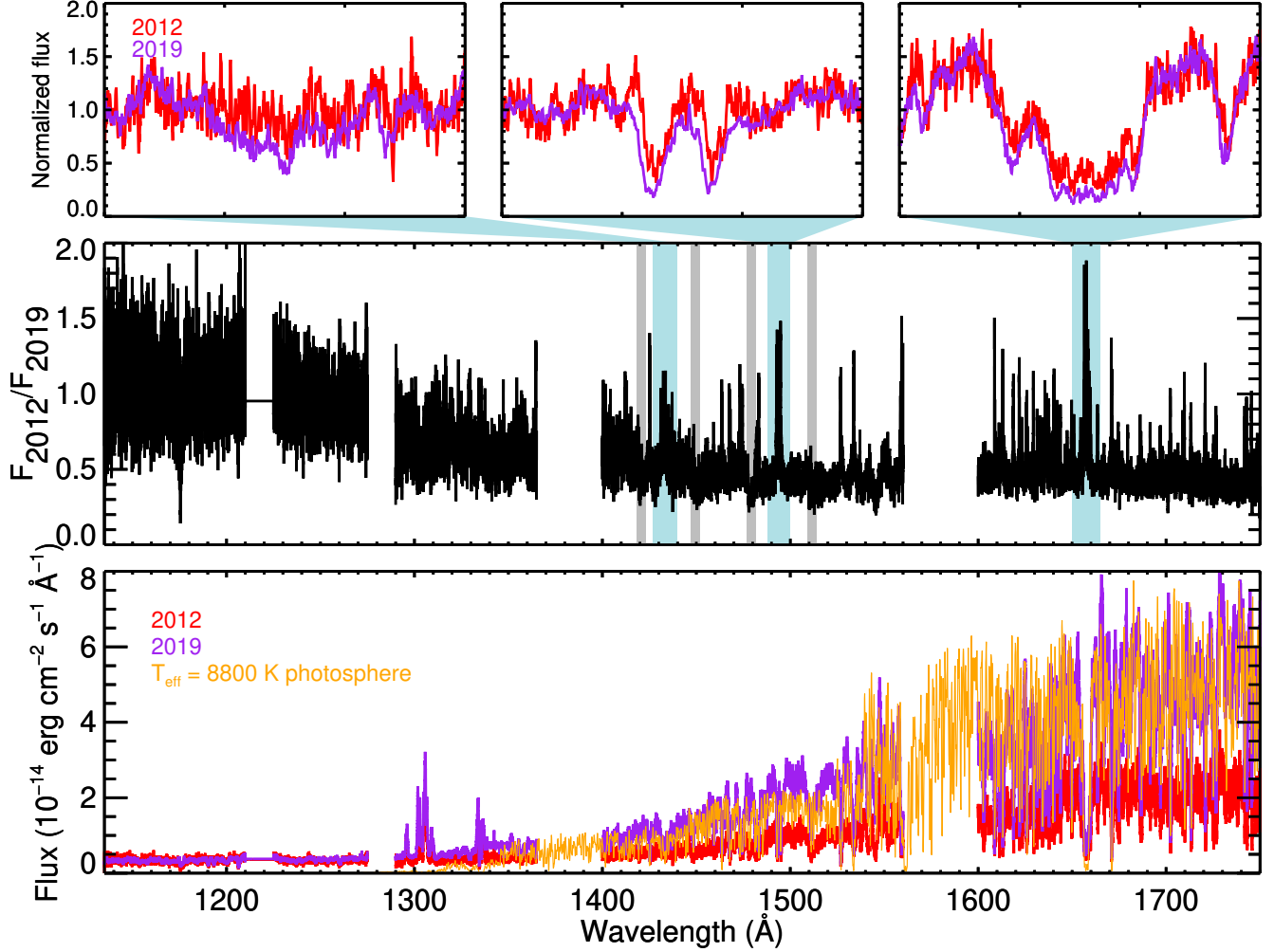


Figure 11. Comparison of the 2012 (red) and 2019 (purple) FUV T Ori spectra. The bottom panel displays the flux spectra from both epochs, as well as a photospheric template scaled to match the 2019 flux. The Lyman- α emission lines are interpolated over for clarity. Only wavelengths common to both sets of observations are shown. The middle panel shows the ratio of the 2012 spectrum to the 2019 spectrum and the top panels show zoomed-in normalized spectrum comparisons between strong spectral features from each epoch. The CO bandheads are marked with gray shaded regions and the wavelength ranges shown in the top panels are marked with light blue shading in the middle panel.

the viewing geometry for the disk around HK Ori. More precise constraints on our viewing angle through these circumstellar environments could help clarify the interpretation of the large value for the Doppler parameter.

4.4. Spatial Location and Distribution of Molecular Absorption Components around HK Ori

We have measured significant columns of H_2 and CO towards HK Ori. The presence of the K4 companion at $0''.3$ might suggest that the COS observations contain flux from both components. While it is plausible that the less massive companion contributes some coronal emission line flux to the FUV spectrum, the absorption signatures are most likely produced by circumstellar material around the primary: [Smith et al. \(2005\)](#) found

no evidence for an IR excess around the K4 companion whereas the IR excess around HK Ori A is well matched by an accretion disk extending to ≈ 30 AU. Given the lack of circumstellar material around the secondary, we continue under the assumption that the absorption is created by material occulting the primary star.

The most critical assumption necessary for deriving a CO/ H_2 ratio in a disk via pencil beam absorption is that the CO and H_2 populations are co-spatial, i.e., we are sampling the same parcels of the disk in both species. At first glance, the differences in the derived rotational temperatures between the H_2 and CO populations suggest we might be sampling different gas components. However, while the CO rotational levels are populated by collisions, radiative processes can alter the observed

distributions of J -levels. If the local number density is lower than the CO critical density, these levels can radiatively depopulate fast enough that the populations are not representative of the local kinetic temperature.

Referencing the density and temperature structures of Herbig Ae disks presented in Agúndez et al. (2018), we estimate the local H number density in the region probed by our HK Ori H_2 absorption spectra is $n_H \sim 10^{4-7} \text{ cm}^{-3}$. Assuming an H_2 ortho–para ratio of 3 and that the $T_{H_2} \approx T_{kin} = 150 \text{ K}$, the total ortho- + para- H_2 collision rate, summed over all possible lower levels, is $\Gamma_{TOT} = 2.6 \times 10^{-10} \text{ cm}^3 \text{ s}^{-1}$ at $J = 10$ (Yang et al. 2010). The CO critical density for $J = 10$ at 150 K is $n_{H_2} \approx 2.8 \times 10^5 \text{ cm}^{-3}$. Therefore, it is possible that the high- J CO populations that drive the determination of $T(\text{CO})$ are significantly sub-thermal, which would explain the temperature difference between the observed H_2 and CO populations. To explore this possibility, we computed RADEX models (van der Tak et al. 2007) using the online interface². For our measured values of $T(H_2)$, $N(\text{CO})$, b_{CO} , and $n_H = 10^4 \text{ cm}^{-3}$, we find that CO rotational levels $3 \leq J \leq 30$ are characterized by temperatures less than the H_2 rotational temperature. Finally, sub-thermal CO rotational temperatures are almost always observed in co-spatial CO and H_2 populations in the ISM (Burgh et al. 2007; Sheffer et al. 2008). We conclude that while there is uncertainty about the exact spatial distribution of the gas and the viewing geometry, it is reasonable to infer that the H_2 and CO are co-spatial around HK Ori with CO/H_2 ratio $\approx 1.3 \times 10^{-5}$.

The system radial velocity for HK Ori is $\approx 20 - 25 \text{ km s}^{-1}$ (Reipurth et al. 1996; Baines et al. 2004) which means the best-fit radial velocities for both the H_2 and CO absorption are blue-shifted from the system velocity by $\approx 35 - 40 \text{ km s}^{-1}$ since we fit the spectrum in the Earth’s rest frame. Again, it is worth noting that the absolute velocity precision of COS is $\approx 15 \text{ km s}^{-1}$. Even taking into account the velocity precision of COS, the measured blue-shifts for the H_2 and CO absorption are large and inconsistent with a pencil beam observed through a Keplerian disk since material in a circular disk along any line-of-sight should have velocities centered around $\approx 0 \text{ km s}^{-1}$. However, it’s possible that the absorption arises at the base of a molecular disk wind launched magnetocentrifugally from the disk’s upper atmosphere. Evidence of such a wind has been detected in CO emission from the Herbig Ae star HD 163296 by Klaassen et al. (2013) with characteristic velocities of $\approx 18 \text{ km s}^{-1}$. Thus depending on the wind launching angle and the disk inclination angle, blue-shifted velocities of $\approx 40 \text{ km s}^{-1}$ are not unreasonable if the absorption arises in a disk wind.

Given the evidence for a disk or disk wind origin of the gas absorption towards HK Ori, our derived CO/H_2

ratio of $\approx 1.3 \times 10^{-5}$ suggests significant depletion of CO in the circumstellar material relative to the canonical molecular cloud value of 10^{-4} (Bergin & Williams 2017). Lower values of CO/H_2 are expected for cooler disks with mid-plane temperatures $\lesssim 30 - 40 \text{ K}$ which is mainly driven by dust grain surface chemistry (Reboussin et al. 2015). However, the depletion factor of CO is highly dependent on age and location in the disk (e.g., Krijt et al. 2020) which makes it difficult to say anything definitive about HK Ori’s disk based on our derived ratio given the uncertainties around the line-of-sight probed by our observations. If our observations trace the warm molecular layer of HK Ori’s disk, the CO/H_2 ratio is line with the depleted values reported for other protoplanetary disks (e.g., Favre et al. 2013; McClure et al. 2016; Schwarz et al. 2016).

5. CONCLUSION

We presented new FUV observations from the *Hubble Space Telescope* of H_2 and CO absorption towards the Herbig Ae stars HK Ori and T Ori. We find a significant column of CO absorption and a notable lack of H_2 absorption towards T Ori, which we posit is related to variable occultation of the star by inner disk warping. HK Ori shows blue-shifted absorption in both H_2 and CO with derived temperatures and column densities which place the gas firmly in the circumstellar environment around HK Ori. Although there is considerable uncertainty as to the exact line-of-sight traced by our observations, the derived CO/H_2 value around HK Ori is $\approx 1.3 \times 10^{-5}$ suggesting a depleted reservoir of CO. Spatially-resolved molecular emission maps of both systems will help place our pencil-beam observations in context and provide a more precise understanding of the CO/H_2 value derived for the gas around HK Ori.

Acknowledgments: We thank the referee for their suggestions, which helped improve the quality of the manuscript. P. W. C. acknowledges useful conversations with Nicole Arulanantham about the molecular components of inner disks. The data in this paper were obtained through *HST* Guest Observing programs 12996 and 15070. This work has made use of NASA’s Astrophysics Data System and the SIMBAD database, which is operated at CDS, Strasbourg, France.

² <http://var.sron.nl/radex/radex.php>

REFERENCES

- Abgrall, H., & Roueff, E. 1989, *A&AS*, 79, 313
- Ádámkócs, M., Glassgold, A. E., & Najita, J. R. 2014, *ApJ*, 786, 135, doi: [10.1088/0004-637X/786/2/135](https://doi.org/10.1088/0004-637X/786/2/135)
- Agúndez, M., Roueff, E., Le Petit, F., & Le Bourlot, J. 2018, *A&A*, 616, A19, doi: [10.1051/0004-6361/201732518](https://doi.org/10.1051/0004-6361/201732518)
- Alecian, E., Wade, G. A., Catala, C., et al. 2013, *MNRAS*, 429, 1001, doi: [10.1093/mnras/sts383](https://doi.org/10.1093/mnras/sts383)
- Antonellini, S., Banzatti, A., Kamp, I., Thi, W. F., & Woitke, P. 2020, *A&A*, 637, A29, doi: [10.1051/0004-6361/201834077](https://doi.org/10.1051/0004-6361/201834077)
- Baines, D., Oudmaijer, R. D., Mora, A., et al. 2004, *MNRAS*, 353, 697, doi: [10.1111/j.1365-2966.2004.08104.x](https://doi.org/10.1111/j.1365-2966.2004.08104.x)
- Banzatti, A., & Pontoppidan, K. M. 2015, *ApJ*, 809, 167, doi: [10.1088/0004-637X/809/2/167](https://doi.org/10.1088/0004-637X/809/2/167)
- Bergin, E. A., & Williams, J. P. 2017, *The Determination of Protoplanetary Disk Masses*, ed. M. Pessah & O. Gressel, Vol. 445, 1, doi: [10.1007/978-3-319-60609-5_1](https://doi.org/10.1007/978-3-319-60609-5_1)
- Bergin, E. A., Cleeves, L. I., Gorti, U., et al. 2013, *Nature*, 493, 644, doi: [10.1038/nature11805](https://doi.org/10.1038/nature11805)
- Blondel, P. F. C., & Djie, H. R. E. T. A. 2006, *A&A*, 456, 1045, doi: [10.1051/0004-6361:20040269](https://doi.org/10.1051/0004-6361:20040269)
- Bosman, A. D., Walsh, C., & van Dishoeck, E. F. 2018, *A&A*, 618, A182, doi: [10.1051/0004-6361/201833497](https://doi.org/10.1051/0004-6361/201833497)
- Bouret, J. C., & Catala, C. 1998, *A&A*, 340, 163
- Brittain, S. D., Najita, J. R., & Carr, J. S. 2015, *Ap&SS*, 357, 54, doi: [10.1007/s10509-015-2260-4](https://doi.org/10.1007/s10509-015-2260-4)
- Burgh, E. B., France, K., & McCandliss, S. R. 2007, *ApJ*, 658, 446, doi: [10.1086/511259](https://doi.org/10.1086/511259)
- Carr, J. S., & Najita, J. R. 2011, *ApJ*, 733, 102, doi: [10.1088/0004-637X/733/2/102](https://doi.org/10.1088/0004-637X/733/2/102)
- Cauley, P. W., & Johns-Krull, C. M. 2015, *ApJ*, 810, 5, doi: [10.1088/0004-637X/810/1/5](https://doi.org/10.1088/0004-637X/810/1/5)
- Cauley, P. W., Redfield, S., Jensen, A. G., & Barman, T. 2016, *AJ*, 152, 20, doi: [10.3847/0004-6256/152/1/20](https://doi.org/10.3847/0004-6256/152/1/20)
- Cauley, P. W., Redfield, S., Jensen, A. G., et al. 2015, *ApJ*, 810, 13, doi: [10.1088/0004-637X/810/1/13](https://doi.org/10.1088/0004-637X/810/1/13)
- Diplas, A., & Savage, B. D. 1994, *ApJS*, 93, 211, doi: [10.1086/192052](https://doi.org/10.1086/192052)
- Dullemond, C. P., van den Ancker, M. E., Acke, B., & van Boekel, R. 2003, *ApJL*, 594, L47, doi: [10.1086/378400](https://doi.org/10.1086/378400)
- Eidelsberg, M., Jolly, A., Lemaire, J. L., et al. 1999, *A&A*, 346, 705
- Eidelsberg, M., & Rostas, F. 2003, *ApJS*, 145, 89, doi: [10.1086/345596](https://doi.org/10.1086/345596)
- Eiroa, C., Oudmaijer, R. D., Davies, J. K., et al. 2002, *A&A*, 384, 1038, doi: [10.1051/0004-6361:20020096](https://doi.org/10.1051/0004-6361:20020096)
- Espinosa Lara, F., & Rieutord, M. 2011, *A&A*, 533, A43, doi: [10.1051/0004-6361/201117252](https://doi.org/10.1051/0004-6361/201117252)
- Favre, C., Cleeves, L. I., Bergin, E. A., Qi, C., & Blake, G. A. 2013, *ApJL*, 776, L38, doi: [10.1088/2041-8205/776/2/L38](https://doi.org/10.1088/2041-8205/776/2/L38)
- Federman, S. R., Glassgold, A. E., Jenkins, E. B., & Shaya, E. J. 1980, *ApJ*, 242, 545, doi: [10.1086/158489](https://doi.org/10.1086/158489)
- Flaherty, K., Hughes, A. M., Simon, J. B., et al. 2020, *ApJ*, 895, 109, doi: [10.3847/1538-4357/ab8cc5](https://doi.org/10.3847/1538-4357/ab8cc5)
- Flaherty, K. M., Hughes, A. M., Teague, R., et al. 2018, *ApJ*, 856, 117, doi: [10.3847/1538-4357/aab615](https://doi.org/10.3847/1538-4357/aab615)
- Foreman-Mackey, D., Hogg, D. W., Lang, D., & Goodman, J. 2013, *PASP*, 125, 306, doi: [10.1086/670067](https://doi.org/10.1086/670067)
- France, K., Herczeg, G. J., McJunkin, M., & Penton, S. V. 2014a, *ApJ*, 794, 160, doi: [10.1088/0004-637X/794/2/160](https://doi.org/10.1088/0004-637X/794/2/160)
- France, K., Schindhelm, E., Bergin, E. A., Roueff, E., & Abgrall, H. 2014b, *ApJ*, 784, 127, doi: [10.1088/0004-637X/784/2/127](https://doi.org/10.1088/0004-637X/784/2/127)
- France, K., Burgh, E. B., Herczeg, G. J., et al. 2012, *ApJ*, 744, 22, doi: [10.1088/0004-637X/744/1/22](https://doi.org/10.1088/0004-637X/744/1/22)
- Goodman, J., & Weare, J. 2010, *Communications in Applied Mathematics and Computational Science*, 5, 65, doi: [10.2140/camcos.2010.5.65](https://doi.org/10.2140/camcos.2010.5.65)
- Grady, C. A., Perez, M. R., Talavera, A., et al. 1996, *A&AS*, 120, 157
- Haridass, C., & Huber, K. P. 1994, *ApJ*, 420, 433, doi: [10.1086/173573](https://doi.org/10.1086/173573)
- Hein Bertelsen, R. P., Kamp, I., van der Plas, G., et al. 2016, *A&A*, 590, A98, doi: [10.1051/0004-6361/201527652](https://doi.org/10.1051/0004-6361/201527652)
- Hillenbrand, L. A., Strom, S. E., Vrba, F. J., & Keene, J. 1992, *ApJ*, 397, 613, doi: [10.1086/171819](https://doi.org/10.1086/171819)
- Hughes, A. M., Wilner, D. J., Andrews, S. M., Qi, C., & Hogerheijde, M. R. 2011, *ApJ*, 727, 85, doi: [10.1088/0004-637X/727/2/85](https://doi.org/10.1088/0004-637X/727/2/85)
- Husser, T. O., Wende-von Berg, S., Dreizler, S., et al. 2013, *A&A*, 553, A6, doi: [10.1051/0004-6361/201219058](https://doi.org/10.1051/0004-6361/201219058)
- Kama, M., Bruderer, S., van Dishoeck, E. F., et al. 2016, *A&A*, 592, A83, doi: [10.1051/0004-6361/201526991](https://doi.org/10.1051/0004-6361/201526991)
- Klaassen, P. D., Juhasz, A., Mathews, G. S., et al. 2013, *A&A*, 555, A73, doi: [10.1051/0004-6361/201321129](https://doi.org/10.1051/0004-6361/201321129)
- Kochanek, C. S., Shappee, B. J., Stanek, K. Z., et al. 2017, *PASP*, 129, 104502, doi: [10.1088/1538-3873/aa80d9](https://doi.org/10.1088/1538-3873/aa80d9)
- Kreplin, A., Madlener, D., Chen, L., et al. 2016, *A&A*, 590, A96, doi: [10.1051/0004-6361/201628281](https://doi.org/10.1051/0004-6361/201628281)
- Krijt, S., Bosman, A. D., Zhang, K., et al. 2020, *ApJ*, 899, 134, doi: [10.3847/1538-4357/aba75d](https://doi.org/10.3847/1538-4357/aba75d)
- Kriss, G. A. 2011, *Improved Medium Resolution Line Spread Functions for COS FUV Spectra*, COS Instrument Science Report 2011-01(v1)
- Leinert, C., Richichi, A., & Haas, M. 1997, *A&A*, 318, 472

- Long, F., Herczeg, G. J., Pascucci, I., et al. 2017, *ApJ*, 844, 99, doi: [10.3847/1538-4357/aa78fc](https://doi.org/10.3847/1538-4357/aa78fc)
- McCandliss, S. R. 2003, *PASP*, 115, 651, doi: [10.1086/375387](https://doi.org/10.1086/375387)
- McClure, M. K., Bergin, E. A., Cleeves, L. I., et al. 2016, *ApJ*, 831, 167, doi: [10.3847/0004-637X/831/2/167](https://doi.org/10.3847/0004-637X/831/2/167)
- McJunkin, M., France, K., Burgh, E. B., et al. 2013, *ApJ*, 766, 12, doi: [10.1088/0004-637X/766/1/12](https://doi.org/10.1088/0004-637X/766/1/12)
- McJunkin, M., France, K., Schneider, P. C., et al. 2014, *ApJ*, 780, 150, doi: [10.1088/0004-637X/780/2/150](https://doi.org/10.1088/0004-637X/780/2/150)
- Mendigutía, I., Calvet, N., Montesinos, B., et al. 2011a, *A&A*, 535, A99, doi: [10.1051/0004-6361/201117444](https://doi.org/10.1051/0004-6361/201117444)
- Mendigutía, I., Eiroa, C., Montesinos, B., et al. 2011b, *A&A*, 529, A34, doi: [10.1051/0004-6361/201015821](https://doi.org/10.1051/0004-6361/201015821)
- Miotello, A., van Dishoeck, E. F., Kama, M., & Bruderer, S. 2016, *A&A*, 594, A85, doi: [10.1051/0004-6361/201628159](https://doi.org/10.1051/0004-6361/201628159)
- Miotello, A., van Dishoeck, E. F., Williams, J. P., et al. 2017, *A&A*, 599, A113, doi: [10.1051/0004-6361/201629556](https://doi.org/10.1051/0004-6361/201629556)
- Mora, A., Merín, B., Solano, E., et al. 2001, *A&A*, 378, 116, doi: [10.1051/0004-6361:20011098](https://doi.org/10.1051/0004-6361:20011098)
- Muzerolle, J., D'Alessio, P., Calvet, N., & Hartmann, L. 2004, *ApJ*, 617, 406, doi: [10.1086/425260](https://doi.org/10.1086/425260)
- Öberg, K. I., Murray-Clay, R., & Bergin, E. A. 2011, *ApJL*, 743, L16, doi: [10.1088/2041-8205/743/1/L16](https://doi.org/10.1088/2041-8205/743/1/L16)
- Pontoppidan, K. M., Blake, G. A., & Smette, A. 2011, *ApJ*, 733, 84, doi: [10.1088/0004-637X/733/2/84](https://doi.org/10.1088/0004-637X/733/2/84)
- Pontoppidan, K. M., Salyk, C., Blake, G. A., & Käufl, H. U. 2010, *ApJL*, 722, L173, doi: [10.1088/2041-8205/722/2/L173](https://doi.org/10.1088/2041-8205/722/2/L173)
- Reboussin, L., Wakelam, V., Guilloteau, S., Hersant, F., & Dutrey, A. 2015, *A&A*, 579, A82, doi: [10.1051/0004-6361/201525885](https://doi.org/10.1051/0004-6361/201525885)
- Reipurth, B., Pedrosa, A., & Lago, M. T. V. T. 1996, *A&AS*, 120, 229
- Salyk, C., Blake, G. A., Boogert, A. C. A., & Brown, J. M. 2009, *ApJ*, 699, 330, doi: [10.1088/0004-637X/699/1/330](https://doi.org/10.1088/0004-637X/699/1/330)
- Savage, B. D., Bohlin, R. C., Drake, J. F., & Budich, W. 1977, *ApJ*, 216, 291, doi: [10.1086/155471](https://doi.org/10.1086/155471)
- Schwarz, K. R., Bergin, E. A., Cleeves, L. I., et al. 2016, *ApJ*, 823, 91, doi: [10.3847/0004-637X/823/2/91](https://doi.org/10.3847/0004-637X/823/2/91)
- Shappee, B. J., Prieto, J. L., Grupe, D., et al. 2014, *ApJ*, 788, 48, doi: [10.1088/0004-637X/788/1/48](https://doi.org/10.1088/0004-637X/788/1/48)
- Sheffer, Y., Rogers, M., Federman, S. R., et al. 2008, *ApJ*, 687, 1075, doi: [10.1086/591484](https://doi.org/10.1086/591484)
- Sicilia-Aguilar, A., Banzatti, A., Carmona, A., et al. 2016, *PASA*, 33, e059, doi: [10.1017/pasa.2016.56](https://doi.org/10.1017/pasa.2016.56)
- Smith, K. W., Balega, Y. Y., Duschl, W. J., et al. 2005, *A&A*, 431, 307, doi: [10.1051/0004-6361:20041135](https://doi.org/10.1051/0004-6361:20041135)
- Smith, R. L., Pontoppidan, K. M., Young, E. D., & Morris, M. R. 2015, *ApJ*, 813, 120, doi: [10.1088/0004-637X/813/2/120](https://doi.org/10.1088/0004-637X/813/2/120)
- van der Tak, F. F. S., Black, J. H., Schöier, F. L., Jansen, D. J., & van Dishoeck, E. F. 2007, *A&A*, 468, 627, doi: [10.1051/0004-6361:20066820](https://doi.org/10.1051/0004-6361:20066820)
- von Zeipel, H. 1924, *MNRAS*, 84, 684, doi: [10.1093/mnras/84.9.684](https://doi.org/10.1093/mnras/84.9.684)
- Wheelwright, H. E., Oudmaijer, R. D., & Goodwin, S. P. 2010, *MNRAS*, 401, 1199, doi: [10.1111/j.1365-2966.2009.15708.x](https://doi.org/10.1111/j.1365-2966.2009.15708.x)
- Yang, B., Stancil, P. C., Balakrishnan, N., & Forrey, R. C. 2010, *ApJ*, 718, 1062, doi: [10.1088/0004-637X/718/2/1062](https://doi.org/10.1088/0004-637X/718/2/1062)
- Zhang, K., Schwarz, K. R., & Bergin, E. A. 2020, *ApJL*, 891, L17, doi: [10.3847/2041-8213/ab7823](https://doi.org/10.3847/2041-8213/ab7823)